Materials Research. 2021; 24(5): e20210066
DOI: https://doi.org/10.1590/1980-5373-MR-2021-0066

Evaluation of the Synthesis of Zeolite SSZ-13 using Choline Chloride and Different Crystallization Seeds and its Application in the Thermocatalytic Degradation of Ultra-High Molecular Weight Polyethylene

Julyane R. S. Solano[a]*, Raul C. S. Nascimento[a], David C. M. Silva[a], Diogo P. S. Silva[a], Lenivaldo V. Sousa[a], Bruno J. B. Silva[a], Soraya L. Alencar[a], Maritza M. Urbina[a], Paulo H. L. Quintela[b], Antonio O. S. Silva[a]

[a]*Universidade Federal de Alagoas, Departamento de Engenharia Química, Laboratório de síntese de catalisadores, Maceió, AL, Brasil.*
[b]*Universidade Federal de Sergipe, Departamento de Engenharia Química, São Cristóvão, SE, Brasil.*

Received: January 25, 2021; Revised: May 24, 2021; Accepted: June 30, 2021

The synthesis of SSZ-13 was studied by evaluating the influence of two types of crystallization seeds with CHA structure (S_1 seeds prepared in fluoride medium and S_2 seeds by the conversion of zeolite Y), SiO_2/Al_2O_3 (28, 40, 60 and 100) and OH/SiO_2 (0.6 and 0.8) ratios. Choline chloride was used as the structure-directing agent and the crystallizations occurred at 140 ºC from 24 to 96 h. S_1 seeds led to the coexistence of zeolites SSZ-13 and P, while S_2 seeds promoted in all SiO_2/Al_2O_3 ratios and OH/SiO_2 = 0.8, the formation of pure SSZ-13 after 24 h. The SSZ-13 samples are formed by clusters of crystals with cuboid-like morphology and exhibited textural properties typical of CHA framework. SSZ-13 zeolite led to a decrease in the temperature and the activation energy required for the degradation of ultra-high molecular weight polyethylene polymer, demonstrating its efficiency as catalyst in this process.

Keywords: *Zeolite SSZ-13, Crystallization seeds, Choline chloride, Ultra-high molecular weight polyethylene, Thermocatalytic degradation.*

1. Introduction

Zeolite SSZ-13 (framework type code CHA, with SiO_2/Al_2O_3 ratio > 6) has a three-dimensional structure formed by 4-, 6- and 8-membered ring (MR), containing large cages (0.73 nm) and intersecting channels with a diameter of 0.38 nm[1,2]. Due to some properties presented by SSZ-13, such as large specific surface area, high ion-exchange capacity, strong surface acidity, remarkable molecular-shape selectivity and thermal/hydrothermal stability, several studies report the application of this material in adsorption processes and CO_2 separation[3-5], conversion of methanol to olefins (MTO), in which it can increase the yield of low-carbon olefins[6-9], in the selective catalytic reduction (SCR) of NO_x[10-13] and pyrolysis of low-density polyethylene (LDPE)[14].

Crystallization of SSZ-13 has been carried out using different methodologies, the main ones being the direct synthesis (from silica and alumina precursors) and the conversion of zeolite Y[1]. The first synthesis of SSZ-13 was reported by Zones in 1985[15]. However, the application of this material initially became limited due to the use of expensive organic structure-directing agents (SDAs)[16], such as N,N,N-trimethyl-1-adamantammonium hydroxide (TMAdaOH) and N,N,N-trimethyl-1-adamantammonium iodide, making its synthesis costly and with low solid yields[17-20]. In view of this, studies were focused on optimizing the synthesis of SSZ-13, in order to make its production economically attractive. Different organic molecules, like tetraethyl phosphonium hydroxide (TEPOH)[21], copper-tetraethylenepentamine (Cu-TEPA)[22-24], tetraethylammonium hydroxide (TEAOH)[25,26], benzyltrimethylammonium hydroxide (BTMAOH)[27] and choline chloride[28,29] were reported as structure-directing agents to synthesize zeolite SSZ-13.

Different procedures have been described to obtain the chabazite structure (CHA) from the conversion of zeolite Y (as a source of Si and Al), which decomposes/dissolves and generates ordered aluminosilicate species, that are subsequently rearranged to form another zeolitic structure[27]. Martín et al.[25] described the combination of zeolite Y with TEAOH, resulting in chabazite being obtained after 72 h of crystallization. However, these routes present as a major disadvantage the long crystallization period, around 3 to 5 days.

The addition of seed crystals of the desired zeolite phase in the synthesis gel generally leads to a faster consumption of reagents and/or secondary nucleation mechanism[30], resulting in higher crystallization rates[31-34] as well as allowing control of the crystal size distribution[35]. The use of crystallization seeds combined with a less expensive structure-directing agent is one of the alternatives to produce the SSZ-13 with shorter times, which makes the synthesis more economical and with greater potential for industrial application.

*e-mail: *julyane.rocha@hotmail.com*

Therefore, it is desirable to develop more efficient routes to synthesize SSZ-13, in order to meet the growing interest in high quality catalysts and enable new applications for this material. In the present work, the synthesis of zeolite SSZ-13 was investigated from reaction mixtures with different SiO_2/Al_2O_3 and OH/SiO_2 ratios, using choline chloride as structure-directing agent and two types of crystallization seeds (with CHA structure) obtained by different methodologies. The synthesized samples were then evaluated in the thermocatalytic degradation of ultra-high molecular weight polyethylene (UHMWPE).

2. Experimental

2.1. Reagents

The following reagents were used in the experiments: ammonium fluoride (Sigma-Aldrich, 98%), potassium hydroxide (Sigma-Aldrich, 85%), aluminum hydroxide (Merck, 63%), colloidal silica (Ludox AS-40, Sigma-Aldrich), sodium aluminate (Sigma-Aldrich, 98%), choline chloride (Sigma-Aldrich, 98%) and ammonium nitrate (Merck, 99%).

2.2. Synthesis of the crystallization seeds

S_1 seeds synthesis: The S_1 seeds were prepared based on the methodology described by Liu et al.[36], with modifications. The molar composition of the synthesis mixture was: $1.0SiO_2{:}0.2Al_2O_3{:}0.39K_2O{:}0.3NH_4F{:}35.0H_2O$ The preparation procedure of the synthesis mixture was as follows: (i) dissolution of ammonium fluoride in 50% of the distilled water required for the synthesis; (ii) dissolution of potassium hydroxide in the remaining distilled water, followed by the addition of aluminum hydroxide; (iii) the solutions obtained in steps (i) and (ii) were mixed together; (iv) then, the colloidal silica was added to the mixture obtained in step (iii). During steps (i) to (iv) mechanical stirring (400 rpm) was used for 15 min. The resulting synthesis mixture remained under mechanical stirring at 400 rpm for 4 h and was subsequently transferred to polytetrafluoroethene (PTFE) vessels and sealed in stainless steel autoclaves. The crystallization was carried out in a convection oven at 160 ºC for 72 h, under static conditions. The solids were recovered by vacuum filtration, washed with distilled water until the filtrate reached neutral pH and then dried in an oven at 120 °C for 12 h.

S_2 seeds synthesis: The S_2 seeds were synthesized based on the study by Bourgogne et al.[37]. The following procedure was performed: (i) dissolution of potassium hydroxide in the distilled water required for the synthesis; (ii) adding zeolite faujasite (Zeolyst International, CBV 500) to the solution obtained in step (i). The resulting mixture was stirred for 5 min to form a synthesis mixture with molar composition $1.0SiO_2{:}0.2Al_2O_3{:}0.4\ {}_2O{:}44.8H_2O$, which was then divided and transferred to PTFE-lined stainless steel autoclaves. The synthesis was carried out in a convection oven at 95 ºC for 72 h, under static conditions. The steps of recovery, washing and drying of the solids were conducted as described for the S_1 seeds.

2.3. Synthesis of zeolite SSZ-13

Zeolite SSZ-13 was synthesized according to the methodology described by Xu et al.[28], with some modifications. Choline chloride (CC) was used as structure-directing agent and the mass of seed crystals was fixed at 10% of the SiO_2 mass. The molar composition of the synthesis mixture was: $0.125CC{:}1.0SiO_2{:}xAl_2O_3{:}yNa_2O{:}12H_2O$, with $x = 0.0357$, 0.025, 0.0167 or 0.0128 and y = 0.3 or 0.4. The reaction mixture was prepared through the following steps: (i) dissolution of sodium hydroxide and sodium aluminate in 80% of the distilled water required for the synthesis (ii) addition of choline chloride in the solution obtained in step (i); (iii) addition of colloidal silica in the mixture resulting from step (ii); iv) The seeds (S_1 or S_2) were dispersed in the remaining water and then were added to the mixture obtained in step (iii). The mixtures obtained in each step were submitted to mechanical stirring (400 rpm) for 15 min, except for (iii), in which the stirring time was 40 min. Then, the resulting gel was divided and transferred to PTFE-lined stainless steel autoclaves, which were heated in a convection oven at 140 ºC for 24 to 96 h, under static conditions.

After crystallization, the solids were separated from the supernatant liquid by vacuum filtration, washed with distilled water until the filtrate reached neutral pH, and then dried in an oven at 120 °C for 12 h. Then, the samples were calcined at 550 °C for 8 h at a heating rate of 2 °C min^{-1}, under a synthetic air flow of 100 mL min^{-1}. Subsequently, the materials were subjected to ion exchange using a 0.1 mol·L^{-1} ammonium nitrate solution at 80 °C for 12 h (1 g of solids per 100 mL of solution). Finally, the samples were again dried and calcined, under the same conditions previously described.

The solid yield was determined by weighing the synthesis mixture and the final dry solids. The yield was calculated on a dry basis, i.e., discounting the mass of water added in the reaction mixture, using Equation 1.

$$\text{Yield}(\%) = \frac{\text{Mass of the final solid}}{\text{Mass of synthesis mixture on a dry basis}} \text{ X } 100 \quad (1)$$

2.4. Characterization

X-ray diffractometry (XRD) was performed using a Shimadzu XRD-6000 diffractometer, with CuKα radiation ($\lambda = 0.15418$ nm), Ni filter, 40 kV voltage and 30 mA current intensity. Data were collected in the 2θ range between 3 and 40º, with goniometer speed of 2º·min^{-1} and step of 0.02º. The area of the diffraction peaks located in the 2θ regions of 8.26° - 10.16°, 19.90° - 21.20° and 29.88° - 31.78° were used to calculate the crystallinity of the materials. Energy dispersive X-ray spectroscopy (EDX) was conducted on a Shimadzu EDX-7000/8000 spectrometer to determine the SiO_2/Al_2O_3 ratio of the samples. Thermal analysis (TG/DTG) was carried out in a Shimadzu DTG-60H thermobalance, using alumina pans and sample masses of approximately 10 mg. The samples were heated from 30 to 800 ºC at a rate of 10 ºC·min^{-1}, in a dynamic atmosphere of synthetic air (flow rate of 50 mL·min^{-1}). Nitrogen adsorption-desorption measurements were performed using a Micromeritics ASAP 2020 equipment at -196 ºC, in the relative pressure range between (P/P_0) between 0.01 and 0.99. The solids were previously degassed at 350 ºC for 12 h, under vacuum of 2 μmHg. The specific surface area (S_{BET}) was calculated using the BET method. The microporous area (S_{Micro}), external

surface area (S_{Ex}) and microporous volume (V_{Micro}) were determined by the t-plot method. The total pore volume (V_T) was measured using the single-point BET method at P/P_0 = 0.975. Scanning electron microscopy (SEM) was carried out using a Shimadzu SSX-550 electron microscope. Temperature-programmed desorption of ammonia (NH_3-TPD) was conducted in a multipurpose reaction system (SAMP3 model equipment, Termolab - Brazil) equipped with thermal conductivity detector. In these measurements, a mass of approximately 100 mg of sample was submitted to a pretreatment at 400 °C for 1 h, under helium atmosphere with a flow rate of 30 mL·min^{-1} Then, the temperature was reduced to 100 °C and the sample was kept in contact with the ammonia stream at a flow rate of 30 mL·min^{-1} for 40 min. The next step of the process was the removal of the physisorbed NH_3 molecules at 100 °C for 1 h, under a helium flow rate of 30 mL min^{-1}. Finally, the NH_3 desorption curves were obtained in the temperature range between 100 and 800 °C, with a heating rate of 10 °C min^{-1} and under helium flow rate of 30 mL min^{-1}.

2.5. Thermocatalytic degradation of UHMWPE

Ultra-high molecular weight polyethylene (UHMWPE, Sigma-Aldrich) was used in the thermocatalytic degradation tests. The catalysts were previously dried in an oven at 100 °C for 12 h and then mixed with UHMWPE using an agate mortar, in the proportion by weight of 30% catalyst/70% polymer, based on the study described by Silva et al.[38]. The mixtures were dried in an oven at 100 °C for 4 h before each analysis. The polymer thermocatalytic degradation experiments were carried out in a Shimadzu DTG-60H thermobalance, from room temperatures to 1000 °C, under nitrogen flow of 50 mL·min^{-1} and heating rates of 10, 20 and 40 °C min^{-1}. Approximately 10 mg of sample were used in each test. From the obtained data, the activation energy of the degradation reaction of UHMWPE with and without catalyst was determined, using the Flynn-Wall-Ozawa non-isothermal kinetic model[39-41].

3. Results and Discussion

3.1. Physicochemical Characterization

The synthesis conditions and the results of XRD and EDX characterizations are shown in Table 1.

The EDX results revealed that the samples composed only by SSZ-13 phase (Z13 to Z16) had similar SiO_2/Al_2O_3 ratios (between 8.2 and 8.7), suggesting an optimal range for the formation of well-crystallized zeolite SSZ-13. It can be observed that the increase in the OH/SiO_2 ratio had a strong influence on SSZ-13 crystallization, but on the other hand it promoted significant reductions in solid yield, probably due to the increase in the concentration of silicon in the liquid phase had inhibited the solid formation. During the formation of the aluminosilicate framework, some of the lattice Si^{4+} ions are replaced by Al^{3+}, depending on the SDA content of the mixture. Therefore, the incorporation of aluminum in the lattice generates negative charges that are compensated by inorganic cations (such as sodium, introduced from the

Table 1. Synthesis and characterization results (XRD and EDX).

Sample	Synthesis conditions				[a]Solid yield (%)	Products		
	SiO_2/Al_2O_3 molar ratio	OH/SiO_2 molar ratio	Seeds	Time (h)		[b]SiO_2/Al_2O_3 final molar ratio	[d]Phase	[c]Relative crystallinity (%)
S_1 Seeds	5	1.38	---	72	98	5	Chabazite	79
Z1	28	0.6	S_1	96	63	---	SSZ-13 + Amorphous	8
Z2	40	0.6	S_1	96	48	---	SSZ-13 + Amorphous	16
Z3	60	0.6	S_1	96	20	---	SSZ-13 + Amorphous	17
Z4	100	0.6	S_1	96	9	---	SSZ-13 + Amorphous	67
Z5	28	0.8	S_1	24	35	9,2	SSZ-13 + Zeolite P	79
Z6	40	0.8	S_1	24	20	9,0	SSZ-13 + Zeolite P	50
Z7	60	0.8	S_1	24	14	8,4	SSZ-13 + Zeolite P	48
Z8	100	0.8	S_1	24	13	8,2	SSZ-13 + Zeolite P	56
S_2 Seeds	5	0.813	---	72	80	5	Chabazite	80
Z9	28	0.6	S_2	96	44	---	SSZ-13 + Amorphous	31
Z10	40	0.6	S_2	96	49	---	SSZ-13 + Amorphous	18
Z11	60	0.6	S_2	96	16	---	SSZ-13 + Amorphous	65
Z12	100	0.6	S_2	96	17	---	SSZ-13 + Amorphous	81
Z13	28	0.8	S_2	24	41	8,3	SSZ-13	100
Z14	40	0.8	S_2	24	30	8,2	SSZ-13	94
Z15	60	0.8	S_2	24	25	8,7	SSZ-13	99
Z16	100	0.8	S_2	24	15	8,4	SSZ-13	98

[a] Obtained by equation 1. [b] Determined by EDX – The estimated values may have errors of up to ±10%.[c] Determined by XRD.

mineralizing agent NaOH) and organic cations (such as choline, which is the SDA used in the synthesis). Thus, depending on these factors, the crystallization of the SSZ-13 zeolite can generate materials with a particular range of Si/Al molar ratio[42].

The XRD profiles of the crystallization seeds and of the samples containing the SSZ-13 phase with high relative crystallinity are illustrated in Figure 1. The diffractograms of the S_1 and S_2 seeds demonstrate the formation of well-crystallized materials with the main peaks coinciding with those of the CHA structure (JCPDS card 34-137)[27,28], indicating that both methods of preparation employed were effective in the synthesis of such material.

The samples synthesized from both types of seeds and OH/SiO_2 ratio = 0.6 consisted of amorphous materials with small diffraction peaks related to the crystallization seeds themselves. With the increase of the SiO_2/Al_2O_3 ratio of the reaction mixture, samples with partially crystallized SSZ-13 phase were obtained. The increase of the OH/SiO_2 ratio to 0.8, in the presence of S_1 seeds, led to the formation of mixtures of zeolites SSZ-13 and P (JCPDS card 40-1464)[43].

On the other hand, Z13 to Z16 samples synthesized from S_2 seeds exhibited all the diffraction peaks characteristic of zeolite SSZ-13[25,27,44] and higher relative crystallinity after 24 h of crystallization (Table 1). Samples Z13 to Z15 presented a small shoulder referring to the zeolite P at the diffraction peak corresponding to the crystallographic plane (1 0 -1), which is indicative of low concentration contamination (traces of zeolite P). However, this additional peak disappeared after calcination, indicating the low thermal stability of the impurity phase. Thus, under the studied conditions, the type of seed used affected the crystallization time necessary to reach maximum crystallinity and inhibited contamination by other phases.

According to Thompson[45], the theory of nucleation and crystal growth from seed crystals establishes that the rate of crystal growth is proportional to the external surface area available in the seeds. The results obtained for the samples synthesized with the S_2 seeds can be explained by the fact that these seeds have smaller crystals (see SEM results), which in turn exhibit a larger external surface area.

Figure 2 shows the results of the thermal analysis carried out on the most crystalline and contaminant-free SSZ-13 samples (Z13 to Z16). In all cases, thermogravimetric (TG) curves and their respective derivative (DTG) exhibited three distinct mass loss events, which can be attributed to: (i) elimination of surface water and removal of strongly adsorbed water, from ambient temperature to 310 ºC; (ii) oxidative decomposition of choline molecules, between 310 and 510 ºC; (iii) degradation of carbonaceous material (coke) deposited on the sample during the decomposition of the SDA, in the temperature range of 510 to 800 ºC[28]. The percentages of mass loss related to each event are listed in Table 2. The samples showed very similar mass losses, which is in agreement with the analogous results obtained for the relative crystallinity and SAR of the materials presented in Table 1.

The nitrogen adsorption-desorption isotherms of the crystallization seeds and samples Z13 to Z16 are shown in Figures 3 and 4, respectively. All materials presented type I isotherm profiles according to the IUPAC classification, with large amounts of N_2 adsorbed in relative pressures

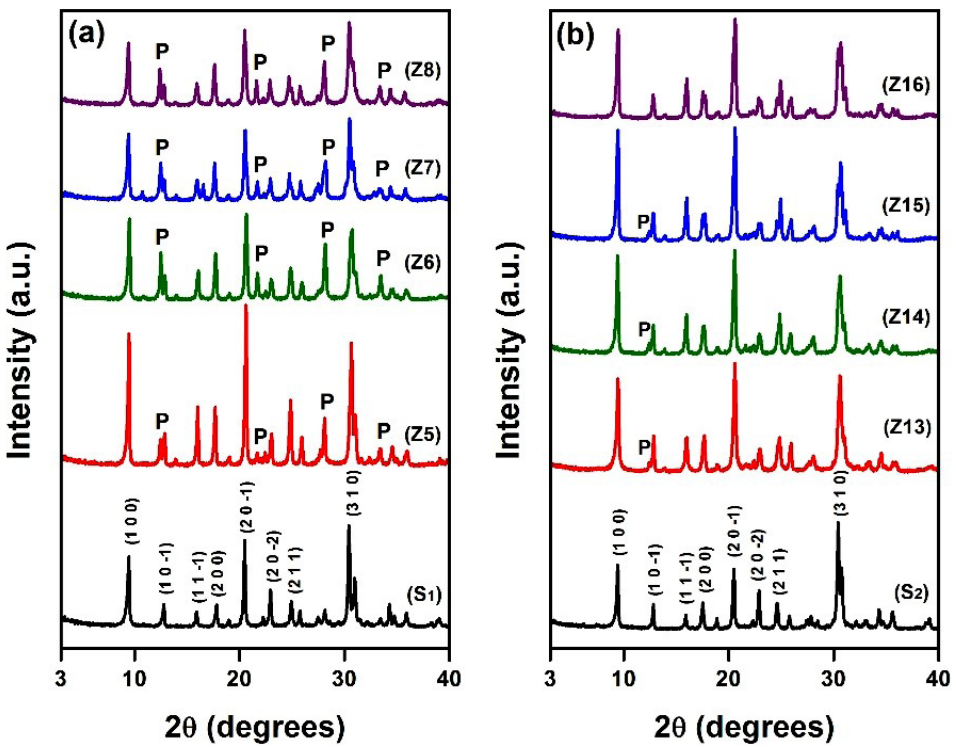

Figure 1. XRD profiles of selected samples synthesized with: (a) S_1 seeds and (b) S_2 seeds. P = Zeolite P phase.

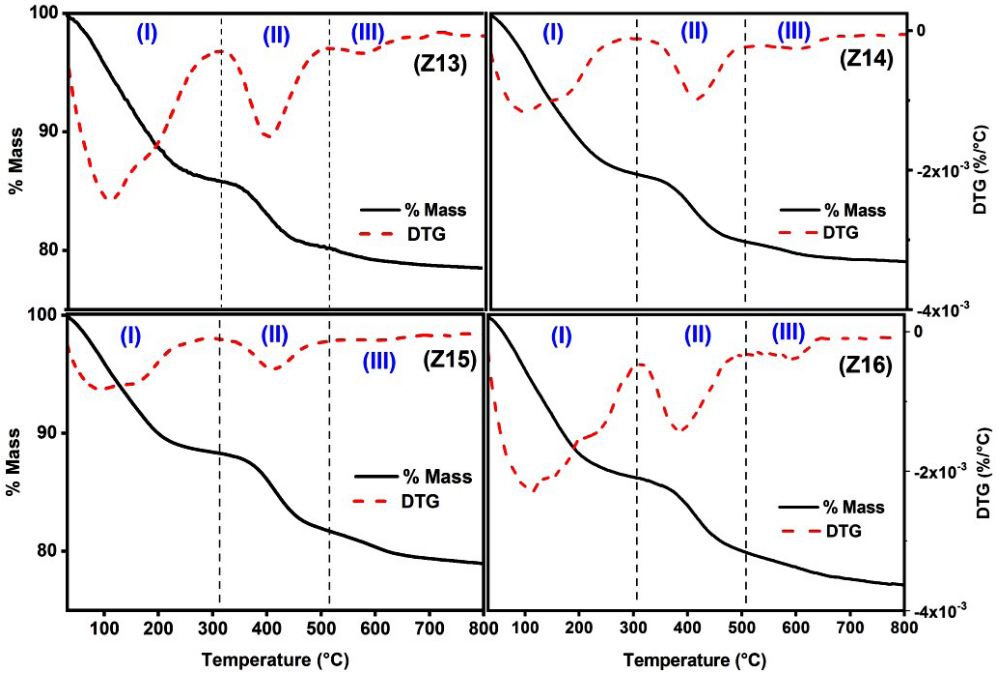

Figure 2. Mass loss profiles from thermal analysis (TG/DTG) of the SSZ-13 samples.

Table 2. Mass loss of the zeolite SSZ-13 samples.

Sample	Mass loss (%) / Temperature range (ºC)			
	(I)	(II)	(III)	Total loss
	30-310 °C	310-510 °C	510-800 °C	(%)
Z13	14.19	5.56	1.85	21.60
Z14	13.66	5.64	1.63	20.93
Z15	11.70	6.44	2.90	21.04
Z16	13.55	6.53	2.88	22.96

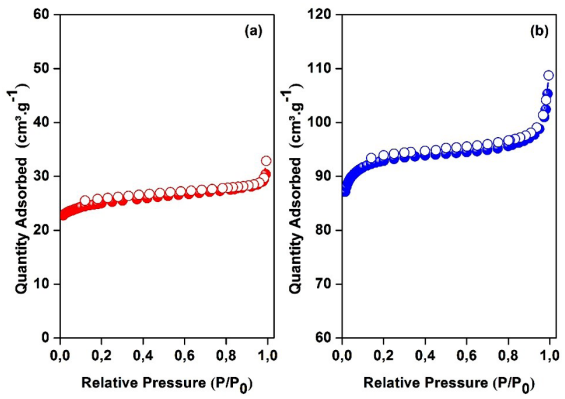

Figure 3. N_2 adsorption-desorption isotherms of the S_1 (a) and (b) S_2 crystallization seeds.

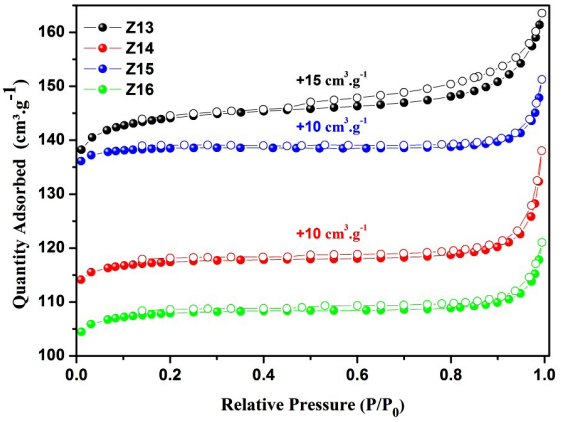

Figure 4. N_2 adsorption-desorption isotherms of the SSZ-13 samples. For clarity, the isotherms were offset along the y axis for Z14 and Z15 (10 $cm^3 \cdot g^{-1}$) and Z16 (15 $cm^3 \cdot g^{-1}$) samples.

$(P/P_0) < 0.1$, in contrast to a low nitrogen uptake in the range of medium to high relative pressures. This indicates that the solids have predominantly narrow micropores (< 1 nm)[46,47]. The low amounts adsorbed by the S_1 and S_2 seeds (Table 3) can possibly be attributed to the existence of K^+ ions in the small 8-ring channels, which strongly hinders nitrogen adsorption[48]. The values of the textural properties of samples Z13 to Z16 determined from the N_2 adsorption-desorption data are listed in Table 3. Samples Z14 and Z16 showed similar values of specific area and microporous volume, while

Table 3. Textural and acidic properties of the seeds and zeolite SSZ-13 samples.

Sample	Textural properties				NH_3–TPD		
	[a]S_{BET}	[b]S_{Ex}	[c]S_{Micro}	[d]V_{Micro}	Weak acid sites	Strong acid sites	Total acid sites
	($m^2.g^{-1}$)	($m^2.g^{-1}$)	($m^2.g^{-1}$)	($cm^3.g^{-1}$)	($\mu mol.g^{-1}$)	($\mu mol.g^{-1}$)	($\mu mol.g^{-1}$)
S_1 Seeds	93	4	89	0.03	---	---	---
S_2 Seeds	117	14	103	0.04	---	---	---
Z13	501	29	472	0.186	812	658	1470
Z14	421	15	406	0.160	671	608	1279
Z15	502	16	486	0.195	945	660	1605
Z16	420	14	406	0.159	662	446	1108

[a]BET surface area. [b]External surface area. [c]Micropore surface area. [d]Micropore volume.

the higher values of these parameters for samples Z13 and Z15 are probably related to their greater crystallinity. The results are in agreement with the relative crystallinity of the materials (Table 1) and with those reported in the literature[1,49].

The TPD-NH_3 profiles of samples Z13 to Z16 in their acid form are illustrated in Figure 5. All catalysts exhibited desorption curves with two main peaks, typical of zeolitic materials[50]. The sharp peak located in the temperature range between 100 and 300 °C can be attributed to the desorption of ammonia weakly bound to the surface that was not removed during the purging step[51-53] and/or from weak Lewis acid sites. On the other hand, the less intense peak observed between 300 and 600 °C is mainly associated with strong Brønsted acid sites[54,55].

The acid sites density values obtained from the NH_3-TPD curves (Table 3) leading to the following acidity order: Z15 > Z13 > Z14 > Z16. The acidity values of the samples were lower than that predicted from the aluminum content in the materials with SAR = 8.5, which is 3171 µmol/g. This fact can be attributed to two simultaneous phenomena: i) the degree of ion exchange of the compensation cations in the synthesized zeolites (Na^+) for ammonium ions (NH_4^+), that even being made in triplicate may not have reached a high level of exchange due to factors such as high Al content in the structure and positions of the exchange sites; ii) presence of amorphous impurities in the samples, as well as the existence of structural defects (Al atoms in octahedral coordination, narrowing and blockage of pores, among other anomalies) that limit the diffusion and adsorption of the NH_3 molecules used in the acidity measurement.

The factors that led to variations in the acidity of the samples are the differences in textural properties, such as internal surface area, total pore volume and micropore volume. These parameters can be indicative of zeolite purity, since lower microporous volume values occur due to crystalline defects such as line defects (edge and screw dislocation), pore blockage, intergrowth of impurity phases, etc[56-58]. According to Table 3, samples Z13 and Z15 showed the highest micropore volume values compared to the other materials and, as these catalysts have similar amounts of aluminum, slightly higher acidity values were also observed.

Figures 6 and 7 shows the micrographs of the crystallization seeds and samples Z13 to Z16, respectively. The seeds clearly exhibited different morphologies. The S_1 material, synthesized in fluoride medium, presents a walnut-like shape (particle size around 20 µm), while the S_2 seed consists of

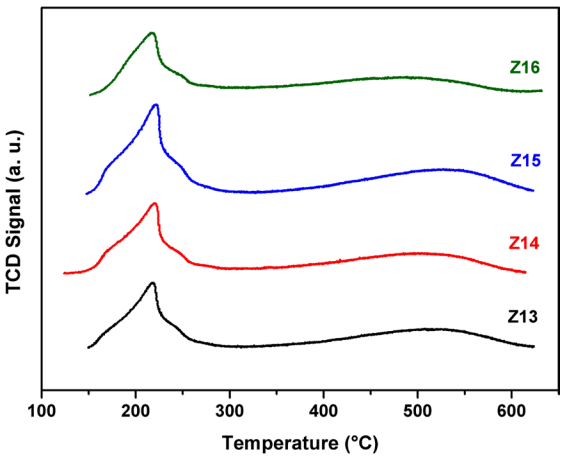

Figure 5. NH_3-TPD profiles of the SSZ-13 samples.

clusters of irregular-shaped particles (< 2 µm). The different morphologies of the two types of seeds are likely due to the different crystallization temperatures (S_1 at 160 °C and S_2 at 95 °C), as well as the use of fluoride to obtain the S_1 seeds, which led to changes in the growth rate of the crystals and consequently a variation in particle sizes[36,59]. The materials synthesized with the aid of S_2 seeds consist of clusters of intergrown particles (< 20 µm), which is a characteristic of seed-assisted syntheses[48]. The Z15 sample is formed by cuboid-like crystals, while the Z13, Z14 and Z16 samples have crystals with an undefined morphology.

3.2. Thermocatalytic degradation of UHMWPE

The mass loss curves of UHMWPE degradation under the heating rate of 10 °C min^{-1} and the activation energy as a function of the conversion in the polymer decomposition process are illustrated in Figure 8. The mass loss curves reveal that the polymer degradation occurred in a single stage, associated with the evaporation or volatilization of light products, and that the addition of the catalysts reduced the decomposition temperature when compared to the purely thermal process. The polymeric macromolecules are broken down on the external surface of the catalyst, where the polymer melts and spreads among the zeolite particles during the degradation process, with the products diffusing through the polymer film or reacting inside the pores[60,61]. The reactions continue through carbocation as transition state,

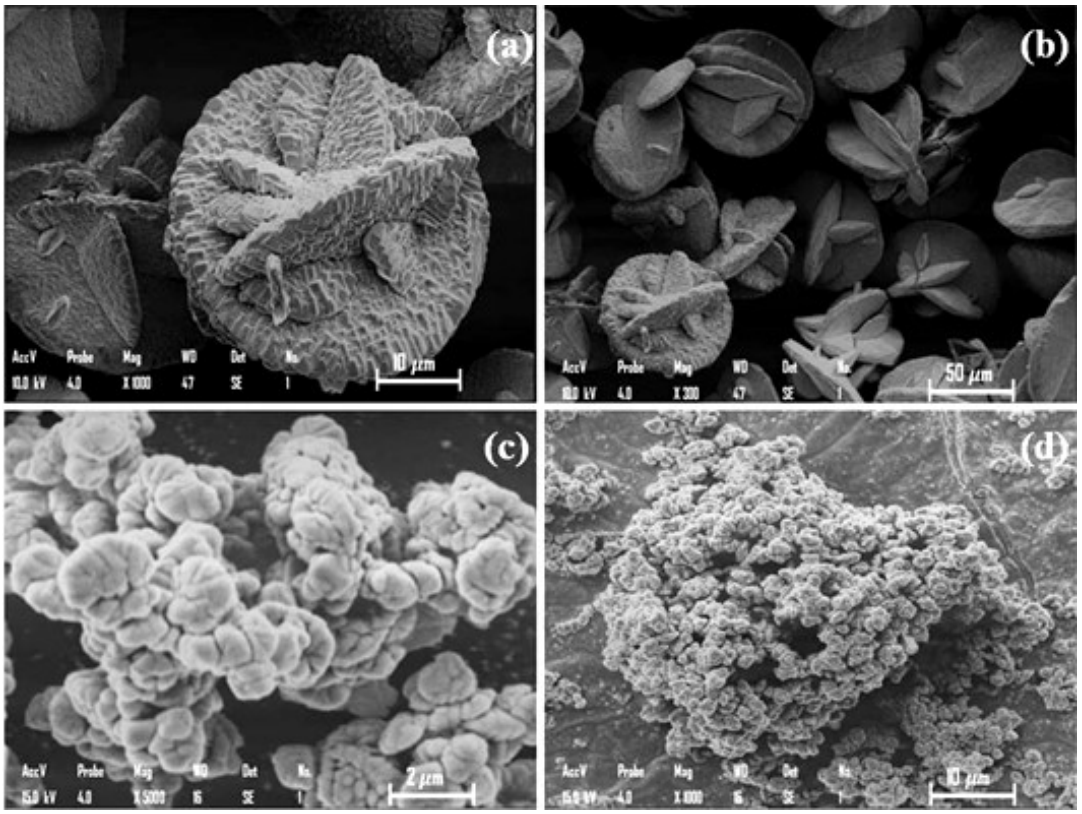

Figure 6. Scanning electron micrographs of the crystallization seeds: (a) and (b) S_1 seeds; (c) and (d) S_2 seeds.

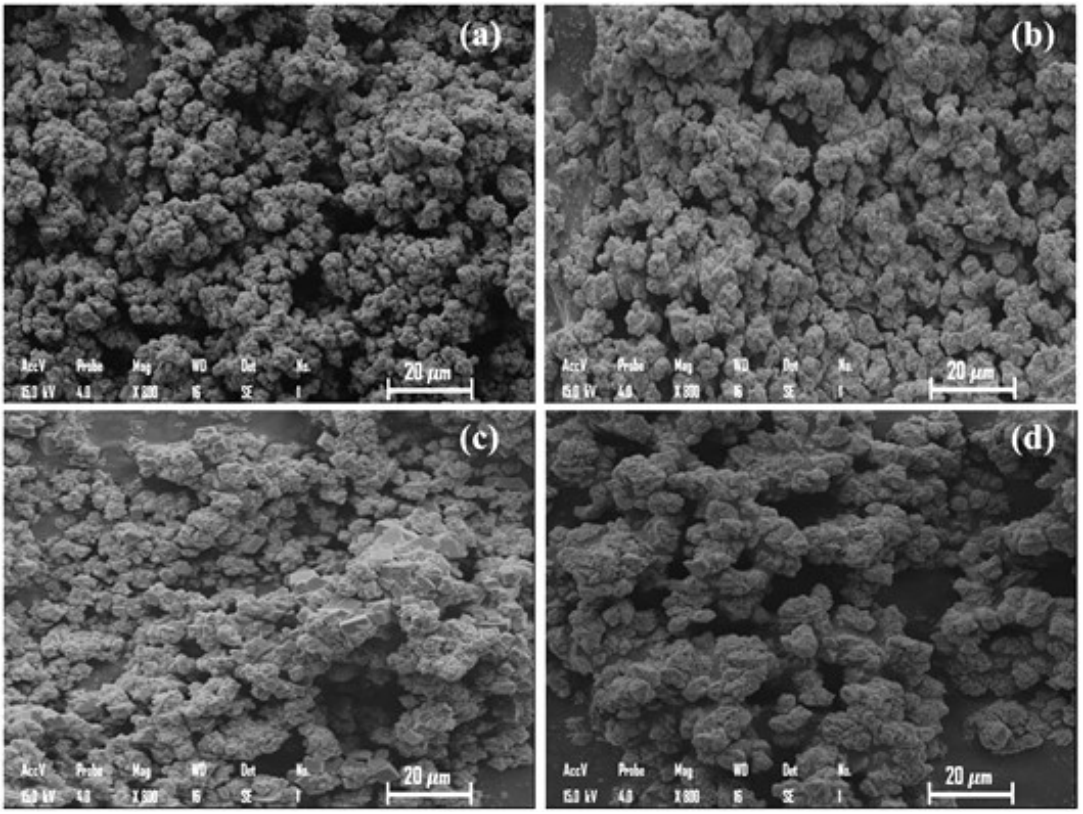

Figure 7. Scanning electron micrographs of the SSZ-13 samples: (a) Z13, (b) Z14, (c) Z15 and (d) Z16.

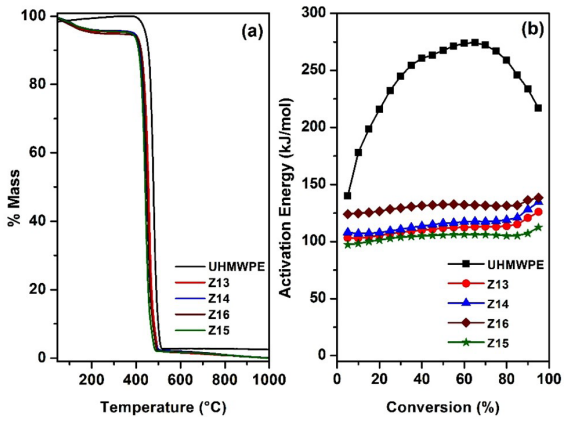

Figure 8. (a) Mass loss curves under the heating rate of 10 °C·min^{-1} and (b) activation energy as a function of the conversion in the UHMWPE degradation process.

which is governed both by the nature of the carbocation and by the type and strength of the acid sites. Thermal degradation occurs through a single reaction mechanism, whereas the presence of acid sites on the catalyst surface leads to the occurrence of different mechanisms[62].

The use of zeolite SSZ-13 significantly reduced the energy level required for polymeric degradation. The Z15 sample showed the lowest activation energy value in the thermocatalytic degradation of UHMWPE compared to the other catalysts, which led to the following average activation energy order (Eam): Z15 (Eam = 104 kJ·mol^{-1}) < Z13 (Eam = 111 kJ·mol^{-1}) < Z14(Eam = 116 kJ·mol^{-1}) < Z16(Eam = 131 kJ·mol^{-1}) < UHMWPE pure (Eam = 241 kJ·mol^{-1}). Fernandes et al.[63] studied the degradation of high-density polyethylene (HDPE) in the presence of natural chabazite and reported average activation energy values of 277.8 kJ·mol^{-1} for the thermal degradation of the polymer and 197.3 kJ·mol^{-1} when using the catalyst. This indicates that zeolites with CHA framework, such as SSZ-13, can act as a catalyst for polymers degradation, enhancing the generation of light products of industrial interest.

4. Conclusions

XRD results showed that the CHA structure was obtained by hydrothermal treatment in fluoride medium (S_1 seeds) and the conversion of zeolite Y (S_2 seeds). The syntheses using choline chloride and S_1 seeds (OH/SiO_2 = 0.8) led to samples with the coexistence of zeolites SSZ-13 and P. On the other hand, pure zeolite SSZ-13 was synthesized after 24 h of crystallization with the aid of the S_2 seeds, indicating a clear effect of the type of seed on the material produced. The EDX results revealed that the samples containing only the zeolite SSZ-13 had SiO_2/Al_2O_3 ratios between 8.2 and 8.7, showing that this material crystallizes with a restricted chemical composition. All materials exhibited type I N_2 adsorption isotherms, typical of microporous materials. NH_3-TPD results showed the following acidity order for the pure SSZ-13 samples: Z15 > Z13 > Z14 > Z16. Slightly higher surface acidity was observed for samples Z13 and Z15 because, in addition to having a similar aluminum content, these materials had the highest micropore volume values. The materials synthesized with the aid of S_2 seeds consist of clusters of intergrown particles (< 20 μm), which is a characteristic of seed-assisted syntheses. The Z15 sample is formed by cuboid-like crystals, while the Z13, Z14 and Z16 samples have crystals with an undefined morphology. The use of SSZ-13 led to a decrease in the temperature and the activation energy required for the degradation of UHMWPE, demonstrating its efficiency as catalyst in the polymer decomposition process.

5. Acknowledgements

The authors are grateful for the financial support provided by Fundação de Amparo à Pesquisa do Estado de Alagoas (FAPEAL), Coordenação de Aperfeiçoamento de Pessoal de Nível Superior (CAPES) and Petrobras.

6. References

1. Sarker M, Khan NA, Yoo DK, Bhadra BN, Jun JW, Kim T-W, et al. Synthesis of SSZ-13 zeolite in the presence of dimethylethylcyclohexyl ammonium ion and direct conversion of ethylene to propylene with the SSZ-13. Chem Eng J. 2019;377:120116.
2. Akporiaye DE, Dahl IM, Mostad HB, Wendelbo R. Aluminum distribution in chabazite: an experimental and computational study. J Phys Chem. 1996;100:4148-53.
3. Liu B, Zhou R, Bu N, Wang Q, Zhong S, Wang B, et al. Room-temperature ionic liquids modified zeolite SSZ-13 membranes for CO_2/CH_4 separation. J Membr Sci. 2016;524:12-9.
4. Hudson MR, Queen WL, Mason JA, Fickel DW, Lobo RF, Brown CM. Unconventional, highly selective CO_2 adsorption in zeolite SSZ-13. J Am Chem Soc. 2012;134:1970-3.
5. Kosinov N, Auffret C, Gücüyener C, Szyja BM, Gascon J, Kapteijnb F, et al. High flux high-silica SSZ-13 membrane for CO_2 separation. J Mater Chem A Mater Energy Sustain. 2014;2:13083-92.
6. Hwang A, Kumar M, Rimer JD, Bhan A. Implications of methanol disproportionation on catalyst lifetime for methanol-to-olefins conversion by HSSZ-13. J Catal. 2017;346:154-60.
7. Li Z, Navarro MT, Martínez-Triguero J, Yu J, Corma A. Synthesis of nano-SSZ-13 and its application in the reaction of methanol to olefins. Catal Sci Technol. 2016;6:5856-63.
8. Wu L, Degirmenci V. Magusin PCMM, Lousberg NJHGM, Hensen EJM. Mesoporous SSZ-13 zeolite prepared by a dual-template method with improved performance in the methanol-to-olefins reaction. J Catal. 2013;298:27-40.
9. Sommer L, Mores D, Svelle S, Stöcker M, Weckhuysen BM, Olsbye U. Mesopore formation in zeolite H-SSZ-13 by desilication with NaOH. Micropor Mesopor Mat. 2010;132:384-94.
10. Han L, Zhao X, Yub H, Hu Y, Li D, Sun D, et al. Preparation of SSZ-13 zeolites and their NH_3-selective catalytic reduction activity. Micropor Mesopor Mat. 2018;261:126-36.
11. Liu Z, Wakihara T, Oshima K, Nishioka D, Hotta Y, Elangovan SP, et al. Widening synthesis bottlenecks: realization of ultrafast and continuous-flow synthesis of high-silica zeolite SSZ-13 for NOx removal. Angew Chem Int. 2015;54:5683-7.
12. Chen B, Xu R, Zhang R, Liu N. Economical way to synthesize SSZ-13 with abundant ion-exchanged Cu^+ for an extraordinary performance in selective catalytic reduction (SCR) of NOx by ammonia. Environ Sci Technol. 2014;48:13909-16.
13. Paolucci C, Verma AA, Bates SA, Kispersky VF, Miller JT, Gounder R, et al. Isolation of the copper redox steps in the standard selective catalytic reduction on Cu-SSZ-13. Angew Chem Int. 2014;53:11828-33.

14. Wardani MK, Kadja GTM, Fajar ATN. Subagjo, Makertihartha IGBN, Gunawan ML, Suendo V, Mukti RR. Highly crystalline mesoporous SSZ-13 zeolite obtained via controlled post-synthetic treatment. RSC Advances. 2019;9:77-87.
15. Zones SI. Zeolite SSZ-13 and its method of preparation. United States patent US 4544538. 1985, Out 1.
16. Shan Y, Shi X, Du J, Yan Z, Yu Y, He H. SSZ-13 Synthesized by Solvent-Free Method: a potential candidate for NH_3-SCR catalyst with high activity and hydrothermal stability. Ind Eng Chem Res. 2019;58:5397-403.
17. Pham TD, Liu Q, Lobo RF. Carbon dioxide and nitrogen adsorption on cation-exchanged SSZ-13 zeolites. Langmuir. 2013;29:832-9.
18. Zones SI. Conversion of faujasites to high-silica chabazite SSZ-13 in the presence of N,N,N-trimethyl-1-adamantammonium iodide. J Chem Soc, Faraday Trans. 1991;87:3709-16.
19. Bohström Z, Arstad B, Lillerud KP. Preparation of high silica chabazite with controllable particle size. Micropor Mesopor Mat. 2014;195:294-302.
20. Hong SH, Jang MS, Cho SJ, Ahn WS. Chabazite and zeolite 13X for CO_2 capture under high pressure and moderate temperature conditions. Chem Commun. 2014;50:4927-30.
21. Yamasaki Y, Tsunoji N, Takamitsu Y, Sadakane M, Sano T. Synthesis of phosphorus-modified small-pore zeolites utilizing tetraalkyl phosphonium cations as both structure-directing and phosphorous modification agents. Micropor Mesopor Mat. 2016;223:129-39.
22. Xie L, Liu F, Ren L, Shi X, Xiao FS, He H. Excellent performance of one-pot synthesized Cu-SSZ-13 catalyst for the selective catalytic reduction of NOx with NH_3. Environ Sci Technol. 2014;48:566-72.
23. Wang J, Peng Z, Qiao H, Han L, Bao W, Chang L, et al. Influence of aging on in situ hydrothermally synthesized Cu-SSZ-13 catalyst for NH_3-SCR reaction. RSC Advances. 2014;4:42403-11.
24. Ren L, Zhu L, Yang C, Chen Y, Sun Q, Zhang H, et al. Designed copper–amine complex as an efficient template for one-pot synthesis of Cu-SSZ-13 zeolite with excellent activity for selective catalytic reduction of NOx by NH_3. Chem Commun. 2011;47:9789-91.
25. Martín N, Moliner M, Corma A. High yield synthesis of high-silica chabazite by combining the role of zeolite precursors and tetraethylammonium: SCR of NOx. Chem Commun. 2015;51:9965-8.
26. Bhadra BN, Seo PW, Khan NA, Jun JW, Kim T-W, Kim C-U, et al. Conversion of Y into SSZ-13 zeolite in the presence of tetraethylammonium hydroxide and ethylene-to-propylene reactions over SSZ-13 zeolites. Catal Today. 2017;298:53-60.
27. Itakura M, Goto I, Takahashi A, Fujitani T, Ide Y, Sadakane M, et al. Synthesis of high-silica CHA type zeolite by interzeolite conversion of FAU type zeolite in the presence of seed crystals. Micropor Mesopor Mat. 2011;144:91-6.
28. Xu R, Zhang R, Liu N, Chen B, Qiao SZ. Template design and economical strategy for the synthesis of SSZ-13 (CHA-type) zeolite as an excellent catalyst for the selective catalytic reduction of NOx by ammonia. Chem Cat Chem. 2015;7:3842-7.
29. Chen B, Xu R, Zhang R, Liu N. Economical way to synthesize SSZ-13 with abundant ion-exchanged Cu+ for an extraordinary performance in selective catalytic reduction (SCR) of NOx by ammonia. Environ Sci Technol. 2014;48:13909-16.
30. Nishi K, Thompson RW. Synthesis of classical zeolites. In: Schüth K, Sing SW, Weitkamp J, editors. Handbook of porous solids. Germany: WILEY-VCH; 2002.
31. Kerr GT. Chemistry of crystalline aluminosilicates. I. Factors affecting the formation of zeolite A. J Phys Chem. 1966;70:1047-50.
32. Kerr GT. Chemistry of crystalline aluminosilicates. IV. Factors affecting the formation of zeolites X and B. J Phys Chem. 1968;72:1385-6.
33. Warzywoda J, Thompson RW. Synthesis of zeolite A in the Na/K system and the effect of seeding. Zeolites. 1991;11:577-82.
34. Lu B, Tsuda T, Oumi Y, Itabashi K, Sano T. Direct synthesis of high-silica mordenite using seed crystals. Micropor Mesopor Mat. 2004;76:1-7.
35. Cundy CS, Forrest JO, Plaisted RJ. 02-O-02-Nucleation processes in zeolite synthesis revealed through the use of different temperature-time profiles. Stud Surf Sci Catal. 2001;135:140.
36. Liu B, Zheng Y, Hu N, Gui T, Li Y, Zhang F, et al. Synthesis of low-silica CHA zeolite chabazite in fluoride media without organic structural directing agents and zeolites. Micropor Mesopor Mat. 2014;196:270-6.
37. Bourgogne M, Guth J-L, Wey R. Process for the preparation of synthetic zeolites and zeolites obtained by said process. United States Patent US 4503024. 1985, Mar 3
38. Silva BJB, Sousa LV, Sarmento LRA, Alencar SL, Quintela PHL, Silva AOS. Kinetic study of thermocatalytic degradation of UHMWPE over microporous and hierarchical ZSM-23 zeolite. Appl Catal B. 2020;267:118699.
39. Flynn JH, Wall LA. General treatment of the thermogravimetry of polymers. J Res Natl Bur Stand, A Phys Chem. 1966;70:487-523.
40. Ozawa T. A new method of analyzing thermogravimetric data. Bull Chem Soc Jpn. 1965;38:1881-6.
41. Ozawa T. A new method of quantitative differential thermal analysis. Bull Chem Soc Jpn. 1966;39:2071-85.
42. Wang Y, Wang C, Wang J, Wang J, Wang L, Xu C, et al. Efficient hydrothermal synthesis of SSZ-13 with variable grain size. Materials. 2020;13(8):1829-43.
43. Hildebrando EA, Andrade CGB, Rocha CAF Jr, Angélica RS, Valenzuela-Diaz FR, Neves RF. Synthesis and characterization of zeolite NaP using kaolin waste as a source of silicon and aluminum. Mater Res. 2014;17:174-9.
44. Wang Y, Chen J, Lei X, Ren Y, Wu J. Preparation of high silica microporous zeolite SSZ-13 using solid waste silica fume as silica source. Adv Powder Technol. 2018;29:1112-8.
45. Thompson RW. Nucleation, growth and seeding in zeolite synthesis. In: Robson H., editor. Verified syntheses of zeolitic materials. London: Elsevier; 2001. p. 21-23.
46. Thommes M, Kaneko K, Neimark AV, Olivier JP, Rodriguez-Reinoso F, Rouquerol J, et al. Physisorption of gases, with special reference to the evaluation of surface area and pore size distribution (IUPAC Technical Report). Pure Appl Chem. 2015;87:1051-69.
47. Wardani MK, Kadja GTM, Fajar ATN, Subagjo, Makertihartha IGBN, Gunawan ML, et al. Highly crystalline mesoporous SSZ-13 zeolite obtained via controlled post-synthetic treatment. RSC Advances. 2019;9:77-87.
48. Zhou RF, Li YQ, Liu B, Hu N, Chen XS, Kita H. Preparation of chabazite membranes by secondary growth using zeolite-T-directed chabazite seeds. Micropor Mesopor Mat. 2013;179:128-35.
49. Leistner K, Xie K, Kumar A, Kamasamudram K, Olsson L. Ammonia desorption peaks can be assigned to different copper sites in Cu/SSZ-13. Catal Lett. 2017;147:1882-90.
50. Katada N, Igi H, Kim JH, Niwa M. Determination of the acidic properties of zeolite by theoretical analysis of temperature-programmed desorption of ammonia based on adsorption equilibrium. J Phys Chem B. 1997;101:5969-77.
51. Lezcano-Gonzalez I, Deka U, Arstad B, Van Yperen-De Deyne A, Hemelsoet K, Waroquier M, et al. Determining the storage, availability and reactivity of NH_3 within Cu-Chabazite-based ammonia selective catalytic reduction systems. Phys Chem Chem Phys. 2014;16:1639-50.

52. Ma L, Cheng Y, Cavataio G, McCabe RW, Fu L, Li J. In situ DRIFTS and temperature-programmed technology study on NH_3-SCR of NOx over Cu-SSZ-13 and Cu-SAPO-34 catalysts. Appl Catal B. 2014;156–157:428-37.
53. Wang D, Gao F, Peden CH, Li J, Kamasamudram K, Epling WS. Selective catalytic reduction of NOx with NH_3 over a CuSSZ-13 catalyst prepared by a solid-state ion-exchange method. Chem Cat Chem. 2014;6:1579-83.
54. Bates SA, Delgass WN, Ribeiro FH, Miller JT, Gounder R. Methods for NH_3 titration of Brønsted acid sites in Cu-zeolites that catalyze the selective catalytic reduction of NO_x with NH_3. J Catal. 2014;312:26-36.
55. Jun JW, Khan NA, Seo PW, Kim CU, Kim HJ, Jhung SH. Conversion of Y into SSZ-13 zeolites and ethylene-to-propylene reactions over the obtained SSZ-13 zeolites. Chem Eng J. 2016;303:667-74.
56. Derouane EG, Védrine JC, Pinto RR, Borges PM, Costa L, Lemos MANDA, et al. The acidity of zeolites: concepts, measurements and relation to catalysis: a review on experimental and theoretical methods for the study of zeolite acidity. Catal Rev. 2013;55(4):454-515.
57. Triantafyllidis KS, Nalbandian L, Trikalitis PN, Ladavos AK, Mavromoustakos T, Nicolaides CP. Structural, compositional and acidic characteristics of nanosized amorphous or partially crystalline ZSM-5 zeolite-based materials. Micropor Mesopor Mat. 2004;75:89-100.
58. Prodingera S, Derewinskib MA. Recent progress to understand and improve zeolite stability in the aqueous medium. Petrol Chem. 2020;60(4):420-36.
59. Subotic B, Broni J. Theoretical and practical aspects of zeolite crystal growth. In: Auerbach SM, Carrado KA, Dutta PK, editors. Handbook of zeolite science and technology. New York: Marcel Dekker Inc; 2003.
60. Marcilla A, Beltrán MI, Navarro R. TG/FT-IR analysis of HZSM5 and HUSY deactivation during the catalytic pyrolysis of polyethylene. J Anal Appl Pyrolysis. 2006;76:222-9.
61. Pinto F, Costa P, Gulyurtlu I, Cabrita I. Pyrolysis of plastic wastes: 2. effect of catalyst on product yield. J Anal Appl Pyrolysis. 1999;51:57-71.
62. Caldeira VPS, Santos AGD, Oliveira DS, Lima RB, Souza LD, Pergher SBC. Polyethylene catalytic cracking by thermogravimetric analysis effects of zeolitic properties and homogenization process. J Therm Anal Calorim. 2017;130:1939-51.
63. Fernandes VJ Jr, Araujo AS, Medeiros RA, Matos JR, Mercuri LP, Silva AOS, et al. Kinetic parameters of polyethylene degradation by the natural zeolite chabazite. J Therm Anal Calorim. 1999;56:1279-82.